Preparation of porcupine-like Bi_2O_3 needle bundles by anodic oxidation of bismuth

Hanna Sopha, Veronika Podzemna, Ludek Hromadko and Jan M. Macak*

Center of Materials and Nanotechnologies, Faculty of Chemical Technology, University of Pardubice, Nam. Cs. Legii 565, 53002 Pardubice, Czech Republic
** e-mail: jan.macak@upce.cz*

Abstract

A new Bi_2O_3 structure resembling bundles of needles was prepared by anodic oxidation of a bismuth substrate in H_2SO_4 electrolyte followed by annealing in air. Needle growth occurred on the timescale of minutes. The resulting porcupine-like needle bundles were characterized using SEM and XRD before and after annealing. The as-grown needles consisted of bismuth aqua sulfate hydroxide; however, upon annealing at 250 °C in air, tetragonal β-Bi_2O_3 was produced without any morphological change.

Keywords

Anodization; bismuth; bismuth oxide, breakdown, needles

1. Introduction

Bi_2O_3 micro- and nanostructures have already been exploited in gas sensors [1], solid oxide fuel cells [2], (photo)catalysis [3,4] and supercapacitors [5]. In order to obtain materials with as large a surface area as possible, much work has been carried out over recent years to prepare nanostructured Bi_2O_3 in the form of nanorods [6], nanoplates [7], nanowires [8], nanopores [9] or nanoparticles [10]. Various approaches have been tried, including hydrothermal methods [6,7], a room-temperature solution synthesis [8], anodic oxidation [9], and gel to crystal conversion [10].

Of these techniques, anodic oxidation is an easy and low-cost method of producing metal oxide films in very short times without extensive instrumentation. Depending on the conditions, nanostructured metal oxide films can be produced, such as nanoporous Al_2O_3 or nanotubular TiO_2 layers [11-13].

Early studies of anodic oxide films on bismuth date back to 1931 [14] and 1957 [15]. More detailed work on the anodic oxidation behavior of bismuth in different solutions was carried out in the early 1960s [16] and 1970s [17,18]. More recently, several attempts have been made to anodize bismuth substrates to produce structures similar to Al_2O_3 or TiO_2. However, bismuth phosphate nanorods [19], non-organized Bi_2O_3 nanoporous films [9,20,21] or thin films consisting of faceted Bi_2O_3 nanoparticles were obtained [22], rather than organized nanoporous or nanotubular layers.

Here we demonstrate for the first time that the facile and quick anodization of bismuth in H_2SO_4 electrolytes results in the robust formation of a completely new type of anodic structure consisting of needles of bismuth aqua sulfate hydroxide that can be easily converted to tetragonal β-Bi_2O_3 needles by annealing in air.

2. Experimental

Bismuth rods with 10 mm diameter (99.997 %, Goodfellow) were cut into round ingots of approx. 5 mm thickness. Bismuth foils (99.97 %, Goodfellow, 50 µm thick on permanent polyester support) that could be easily cut to enable side SEM viewing were also used. Prior to anodization all bismuth substrates were degreased by sonication in isopropanol. The anodizations were carried out in 1 M H_2SO_4, applying a potential of 20 V at a temperature of 5 °C with a sweep rate of 10 V/s. The electrochemical cell consisted of a high-voltage potentiostat (PGU-200V, Elektroniklabor GmbH) in a two-electrode configuration, with a Pt foil as counter electrode and a bismuth substrate as working electrode, pressed against an O-ring of the electrochemical cell, leaving 0.071 cm^2 open to the electrolyte. After anodization the anodized bismuth layers were carefully rinsed with DI water and dried in air. Annealing of the anodized bismuth ingots was carried out in a muffle oven at 250 °C for 1 hour in air.

The structure and morphology of the bismuth layers were characterized by SEM (JEOL JSM 7500F). X-ray diffraction analyses (XRD) were carried out in the micro-diffraction mode with an X-ray diffractometer (Rigaku SmartLab 3kW) using Cu Kα radiation.

3. Results and Discussion

Figure 1(a–c) shows scanning electron microscope (SEM) images of bundles of needles grown on bismuth foils after anodization in 1 M H_2SO_4 at 20 V for 5 min. As can be seen, needles with a diameter of about 250–300 nm were produced over the whole anodized surface. From Figure 1(a) it is clear that the growth of the needle bundles starts at specific

points on the bismuth surface, suggesting that the needles form under conditions of passivity breakdown [23]. The length of the needles ranges from less than ten to dozens of micrometers within each bundle. Figure 1(d) shows a side view of the needle bundles on a bismuth foil with very bulky character. The growth of the bundles proceeds with a significant expansion in volume, which is typical for anodic oxide growth [23-25].

In order to investigate the growth of the needles in more detail, a sequence of anodization runs was carried out exactly as in Figure 1, but with different anodization times. Figure 2 shows low-magnification SEM images of the entire area of bismuth foils anodized for different lengths of time. As can be seen, just after sweeping to 20 V (Figure 2a), no needle bundles had yet appeared. After 30 s (Figure 2b), a number of needle bundles was present on the surface, localized at the breakdown points. After 60 s (Figure 2c), a considerably larger number of needle bundles had grown on the surface. After 5 minutes (Figure 2d), the surface was completely covered by needle bundles. For anodization times longer than 5 minutes, no visual change could be seen on the substrates, except that the overall volume of needles on the substrate gradually increased. However, anodization runs longer than 5 minutes could only be performed on thick bismuth ingots, because the whole volume of a bismuth foil (50 µm thick) was completely converted into needles by anodization.

To assess the mechanism behind the growth of needles, and to investigate the passivity of the bismuth substrates in particular, current densities were monitored during anodization in 1 M H_2SO_4 with either a slow sweep rate or an extremely high sweep rate. Figure 3 shows the polarization behavior (left side) and the current density vs time plot (right side) corresponding to the anodization of bismuth foil in 1 M H_2SO_4 for 5 min at 20 V at a sweep rate of 0.05 V/s (black curve) and at a sweep rate of 10 V/s (red curve).

In the case of slow potential sweep, passivation of the bismuth surface took place, as can be seen from the decrease in the current density after an initial current peak at the beginning of the potential sweep, corresponding to the active dissolution of bismuth. At a potential of approximately 10 V passivation breakdown occurred [26] (as indicated by a black arrow), accompanied by a gradual increase in current over time.

In the case of a fast potential sweep, the current density increased up to a potential of about 10 V and then decreased, which again suggests the passivation of bismuth, although this takes place at higher current densities due to the extremely fast potential increase. When the potential was held constant at 20 V the current density increased again after a few seconds.

At this moment, fast needle growth was initiated, as indicated by a red arrow in Figure 3. The current density then increased until the whole bismuth surface was covered with needle bundles. The current density then decreased again while the thickness of the needle structure increased. As already noted, the 50 µm thick bismuth foils are already anodized over their entire thickness after 5 min. Longer anodization runs can be carried out using bismuth ingots. In this case, the current density decreased to a comparably low steady-state level of about 6 mA/cm^2 after 30 min from the beginning of anodization.

It should be noted that needle growth can also be achieved under slow sweep rates, such as 0.05 V/s as used in Figure 3. However, the needle growth rate is not as high as for fast potential sweeps, and the needle growth itself is less quantitative. The bismuth surface is much less covered than is the case for fast sweep rates, eg 10 V/s as shown in Figure 2 and Figure 3. For fast sweep rates, not only are needle bundles present over the entire surface, but their growth is completed much more quickly, compared to slow sweeping. All in all, faster sweeping leads to more efficient and robust needle synthesis.

Based on the data shown in Figures 1–3 and the visual and acoustic absence of sparks (i.e. this is not a sparking anodization), it can be postulated that the needles grow due to local dielectric breakdown events that take place most likely on defects of the surface of the oxidized bismuth substrate [27]. This hypothesis is supported by the high current densities obtained and the noise due to oxygen bubble evolution (due to the oxidation of water) on the bismuth surface that can be seen in the current density vs time plot. In the course of anodization, more and more defects are available for the current flow. As a consequence, more breakdown events take place (accompanied by further current density increase), so the whole breakdown process shows autocatalytic features. Once the whole surface area is covered with the needle structure the current density decreases.

Figure 4a shows the XRD patterns of the anodized needle bundles on bismuth ingots before (black line) and after (red line) annealing at 250 °C for 1 hour. As can be seen, bismuth aqua sulfate hydroxide ($Bi_2(H_2O)_2(SO_4)_2(OH)_2$) (reference pattern: 01-076-1103) was formed upon anodization. The high bismuth signals that can be seen in the XRD pattern stem from the underlying Bi substrate.

After annealing the anodized bismuth substrate in air, pure tetragonal β-Bi_2O_3 (reference pattern: 00-027-0050) was formed. At this point no bismuth signals can be observed, possibly due to the fact that the crystalline needle bundles have a higher density than amorphous ones (i.e. X-rays do not penetrate the matter so easily) and/or because the bundles might have become overall less porous after annealing (resulting in greater compactness of the bundles,

again more difficult for X-rays to penetrate). Figure 4b shows an SEM image of the anodized and annealed bismuth ingot. It is obvious that the needle structure was maintained after annealing without any morphological change.

Based on these results, the following reaction equations are suggested for the anodization of bismuth in H_2SO_4 (Scheme 1a) and the thermal conversion of the anodic product to β-Bi_2O_3 (Scheme 1b):

a) $2\ Bi + 2\ H_2SO_4 + 4\ H_2O \xrightarrow[25°C]{\Delta U} Bi_2(H_2O)_2(SO_4)_2(OH)_2 + 4\ H^+ + 4\ e^-$

b) $Bi_2(H_2O)_2(SO_4)_2(OH)_2 \xrightarrow[250°C]{Air} Bi_2O_3 + 3\ H_2O + 2\ SO_2$

4. Conclusions

In summary, it was shown that the anodization of bismuth in 1 M H_2SO_4 results in local breakdown of the bismuth surface and the formation of needle bundles consisting of bismuth aqua sulfate hydroxide. After annealing β-Bi_2O_3 was formed while the needle morphology was maintained. Due to their huge surface area, these Bi_2O_3 needles have potential applications in gas sensors, solid oxide fuel cells, (photo)catalysis and supercapacitors.

Acknowledgements

European Research Council (project nr. 638857) and Ministry of Youth, Education and Sports of the Czech Republic (projects nr. LM2015082, CZ.02.1.01/0.0/0.0/16_013/0001829) are acknowledged for financial support of this work. We thank Prof. Tomas Wagner for Bi substrates.

Figure captions

Fig. 1. SEM images showing top (a–c) and side (d) views of the needle bundles obtained by anodization of bismuth foil at 20 V for 5 min in 1 M H_2SO_4 (sweep rate 10 V/s).

Fig. 2. Low-magnification SEM images of bismuth foils anodized at 20 V (sweep rate 10 V/s) for anodization times of: (a) 0 s (just sweeping), (b) 30 s, (c) 60 s and (d) 300 s, showing macroscopically the growth of needle bundles over time. The dashed circles indicate the anodized areas. All scale bars show 1 mm.

Fig. 3. Polarization plot (left) and current transients (right) recorded during the anodization of bismuth foil in 1 M H_2SO_4 at 20 V for 5 min with a sweep rate of 0.05 V/s (black) and 10 V/s (red).

Fig. 4. (a) XRD patterns of needle bundles on a Bi ingot (anodized at 20 V for 30 min) before and after annealing at 250 °C; (b) SEM image of the annealed needle bundles of tetragonal β-Bi_2O_3.

Scheme 1. (a) Anodic oxidation of Bi in H_2SO_4 electrolyte, (b) thermal oxidation of the anodic product to β-Bi_2O_3.

References

[1] A. Cabot, A. Marsal, J. Arbiol, J.R. Morante, Bi_2O_3 as a selective sensing material for NO detection, Sens. Actuators, B 99 (2004) 74-89.

[2] A.M. Azad, S. Larose, S. A. Akbar, Review – Bismuth oxide-based solid electrolytes for fuel cells, J. Mater. Sci. 29 (1994) 4135-4151.

[3] H. Weidong, Q. Wei, W. Xiaohong, D. Xianbo, C. Long, J. Zhaohua, The photocatalytic properties of bismuth oxide films prepared through the sol–gel method, Thin Solid Films 515 (2007) 5362-5365.

[4] M. Hatano, J.H. Lunsford, The oxidative coupling of methane over bismuth oxide, React. Kinet. Catal. Lett. 45 (1991) 1-6.

[5] T.P. Gujar, V.R. Shinde, C.D. Lokhande, S.-H. Han, Electrosynthesis of Bi2O3 thin films and their use in electrochemical supercapacitors, J. Power Sources 161 (2006) 1479-1485.

[6] A.M Abu-Dief, W.S. Mohamed, α-Bi2O3 nanorods: synthesis, characterization and UV-photocatalytic activity, Mater. Res. Express 4 (2017) 035039.

[7] S.S. Bhande, R.S. Mane, A.V. Ghule, S.-H. Han, A bismuth oxide nanoplate-based carbon dioxide gas sensor, Scripta Mater. 65 (2011) 1081-1084.

[8] X. Gou, R. Li, G. Wang, Z. Chen, D. Wexler, Room-temperature solution synthesis of Bi_2O_3 nanowires for gas sensing application, Nanotechnology 20 (2009) 495501.

[9] X. Lv, J. Zhao, X. Wang, X. Xu, L. Bai, B. Wang, Novel Bi_2O_3 nanoporous film fabricated by anodic oxidation and its photoelectrochemical performance, J. Solid State Electrochem. 17 (2013) 1215-1219.

[10] M.M. Patil, V.V. Deshpande, S.R. Dhage, V. Ravi, Synthesis of bismuth oxide nanoparticles at 100 °C, Mater. Lett. 59 (2005) 2523-2525.

[11] H. Masuda, K. Fukuda, Ordered metal nanohole arrays made by a two-step replication of honeycomb structures of anodic alumina, Science 268 (1995) 1466-1468.

[12] J.M. Macak, H. Tsuchiya, A. Ghicov, K. Yasuda, R. Hahn, S. Bauer, P. Schmuki, TiO_2 nanotubes: Self-organized electrochemical formation, properties and applications, Curr. Opin. Solid State Mater. Sci. 11 (2007) 3-18.

[13] K. Lee, A. Mazare, P. Schmuki, One-dimensional titanium dioxide nanomaterials: nanotubes, Chem. Rev. 114 (2014) 9385-9454.

[14] A. Güntherschulze, H. Betz, Neue Untersuchungen über die elektrolytische Ventilwirkung: II. Die Oxydschicht von Sb, Bi, W, Zr, Al, Zn, Mg, Z. Elektrochem. 37 (1931) 726-734.

[15] V. Cupr, E. Dvorakova, Farbige Schichten an Wismutelektroden, Collection Czechozslov. Chem. Commun. 22 (1957) 305-307.

[16] L. Masing, L. Young, Kinetics of formation of anodic oxide films on bismuth, Can. J. Chem. 40 (1962) 903-920.

[17] I.A. Ammar, M.W. Khalil, Anodic oxidation of bismuth in sulphate, carbonate and hydroxide solutions, Electrochim. Acta 16 (1971) 1601-1612.

[18] I.A. Ammar, M.W. Khalil, Behaviour of bismuth as valve metal in phosphate, borate, benzoate, and tartrate solutions, J. Electroanal. Chem. 32 (1971) 373-386.

[19] M. Yang, N.K. Shrestha, R. Hahn, P. Schmuki, Electrochemical formation of bismuth phosphate nanorods by anodization of bismuth, Electrochem. Solid-State Lett. 13 (2010) C5-C8.

[20] K.C. Chitrada, K.S. Raja, R. Gakhar, D. Chidambaram, Enhanced photoelectrochemical performance of anodic nanoporous β-Bi_2O_3, J. Electrochem. Soc. 162 (2015) H380-H391.

[21] M. Ahila, J. Dhanalakshmi, J. Celina Selvakumari, D. Pathinettam Padiyan, Heat treatment effect on crystal structure and design of highly sensitive room temperature CO_2 gas sensors using anodic Bi_2O_3 nanoporous formed in a citric acid electrolyte, Mater. Res. Express 3 (2016) 105025.

[22] M. Ahila, M. Malligavathy, E. Subramanian, D. Pathinettam Padiyan, Controllable synthesis of α and β-Bi_2O_3 through anodization of thermally evaporated bismuth and its characterization, Solid State Ionics 298 (2016) 23-34.

[23] R. Hahn, J.M. Macak, P. Schmuki, Rapid anodic growth of TiO_2 and WO_3 nanotubes in fluoride free electrolytes, Electrochem. Commun. 9 (2007) 947-952.

[24] S. Berger, J. Kunze, P. Schmuki, D. LeClere, A.T. Valota, P. Skeldon, G.E. Thompson, A lithographic approach to determine volume expansion factors during anodization: Using the example of initiation and growth of TiO_2-nanotubes, Electrochim. Acta 54 (2009) 5942-5948.

[25] S.P. Albu, P. Schmuki, Influence of anodization parameters on the expansion factor of TiO2 nanotubes, Electrochim. Acta 91 (2013) 90-95.

[26]P. Schmuki, From Bacon to barriers: a review on the passivity of metals and alloys, J. Solid State Electrochem. 6 (2002) 145-164.

[27]J.W. Schultze, M.M. Lohrengel, Stability, reactivity and breakdown of passive films. Problems of recent and future research, Electrochim. Acta 45 (2000) 2499-2513.

Figure 1

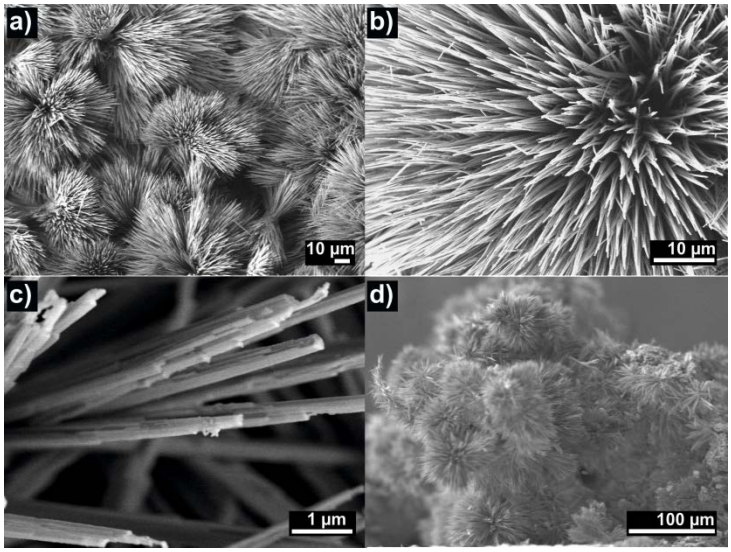

Figure 2

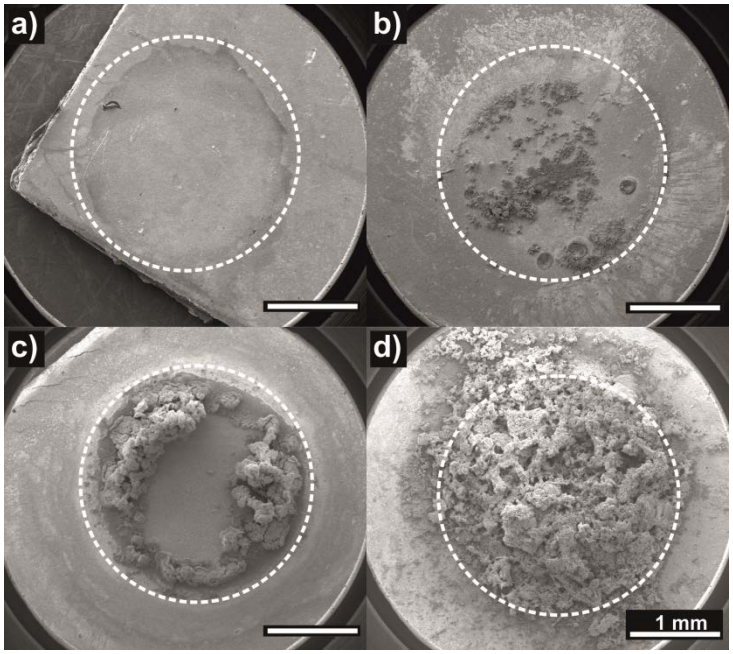

Figure 3

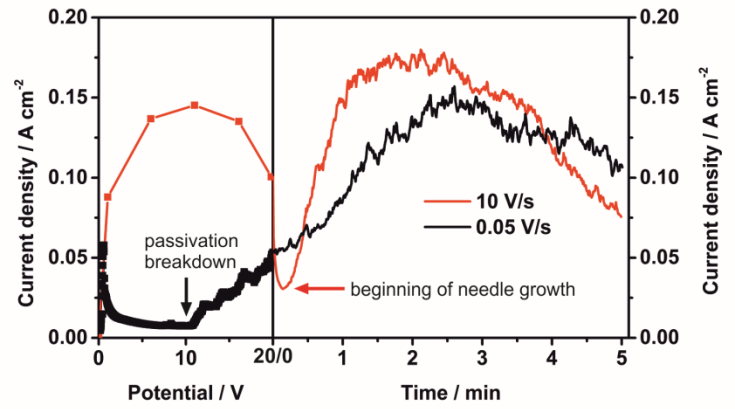

Figure 4

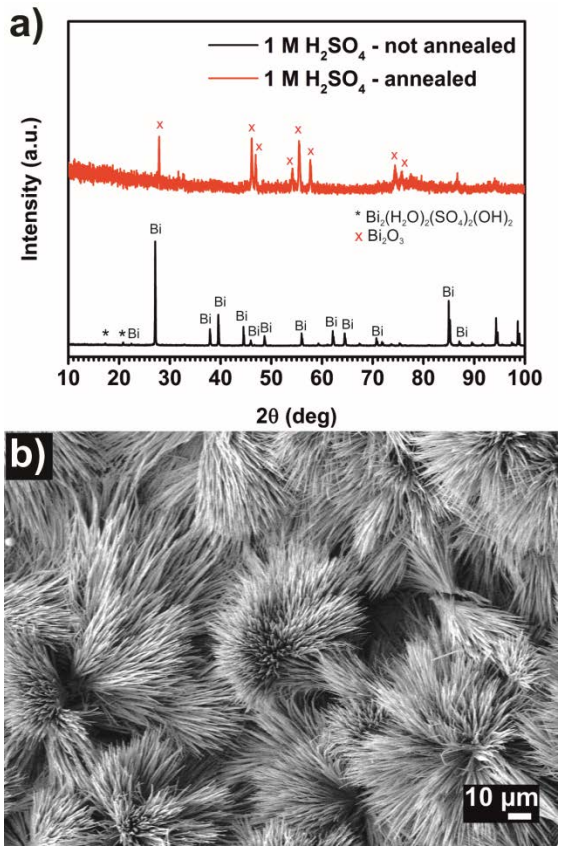

Table of content